

PAPER • OPEN ACCESS

Quantitative Eliashberg theory of the superconductivity of thin films

To cite this article: Giovanni Alberto Ummarino and Alessio Zaccone 2025 *J. Phys.: Condens. Matter* **37** 065703

View the [article online](#) for updates and enhancements.

You may also like

- [Electron-phonon coupling in \$\text{La}_2\text{In}\$ under pressure](#)
Surinder Singh and Udomsilp Pinsook
- [The 2021 room-temperature superconductivity roadmap](#)
Lilia Boeri, Richard Hennig, Peter Hirschfeld et al.
- [Doping dependence and multichannel mediators of superconductivity: calculations for a cuprate model](#)
Fabian Schrodi, Alex Aperis and Peter M Oppeneer

Quantitative Eliashberg theory of the superconductivity of thin films

Giovanni Alberto Ummarino¹  and Alessio Zaccone^{2,3,*} 

¹ Dipartimento di Scienza Applicata e Tecnologia, Politecnico di Torino, Corso Duca degli Abruzzi 24, 10129 Torino, Italy

² Department of Physics 'A. Pontremoli', University of Milan, via Celoria 16, 20133 Milan, Italy

³ Institut für Theoretische Physik, University of Göttingen, Friedrich-Hund-Platz 1, 37077 Göttingen, Germany

E-mail: alessio.zaccone@unimi.it

Received 18 July 2024, revised 28 October 2024

Accepted for publication 14 November 2024

Published 22 November 2024



Abstract

A quantitative theory of the superconductivity of materials confined at the nanoscale in parameter-free agreement with experimental data has been missing so far. We present a generalization, in the Eliashberg framework, of a BCS theory of superconductivity in good metals which are confined along one of the three spatial directions, such as thin films. In this formulation of the Eliashberg equations the approximation of taking the normal density of states as its value at the Fermi level has been removed. By numerically solving these new Eliashberg-type equations, we find the dependence of the superconducting critical temperature T_c on the confinement size L , in quantitative agreement with experimental data of Pb and Al thin films with no adjustable parameters. This quantitative agreement provides an indirect confirmation that, upon increasing the confinement, a crossover from a spherical-like Fermi surface, which contains two growing hole pockets caused by the confinement, to a strongly deformed Fermi surface, occurs. This topology of the Fermi sea is implemented in the new Eliashberg-type equations to reproduce the experimentally observed maximum in the critical superconducting temperature vs film thickness of ultra-thin Pb films.

Keywords: superconductivity, thin films, elemental metals, electron–phonon, Eliashberg theory

1. Introduction

Superconducting thin films are of fundamental interest for physics since they provide a model system to understand the effect of confinement on quantum macroscopic phenomena [1–7]. Also, they play a crucial role in a variety of applications, which include Josephson junctions (Dayem bridges) [8], single-photon detectors for space

telecommunications [9], qubits for quantum computing [10] etc. More recently, the effect of the electric field-driven suppression of superconductivity has been discovered in pioneering works by Giazotto and collaborators on metallic superconducting thin films [11] and superconducting quantum interference devices [12]. This novel supercurrent field effect opens up unprecedented opportunities to fabricate electric field-gated quantum materials. Crucially, the effect leverages the film thickness-dependent suppression of superconductivity under an external electric field [13].

In spite of this being a central topic in contemporary condensed matter and quantum physics, no fully quantitative theory of size-dependent superconductivity in real materials exists to date.

The standard one-infinite-band s-wave Eliashberg theory [14, 15] is a powerful tool to explain exactly all

* Author to whom any correspondence should be addressed.



Original Content from this work may be used under the terms of the [Creative Commons Attribution 4.0 licence](https://creativecommons.org/licenses/by/4.0/). Any further distribution of this work must maintain attribution to the author(s) and the title of the work, journal citation and DOI.

superconductive properties of old low T_c superconductors [15] as Pb, Sn, Al etc. Lately, new experimental data [15] have appeared that seem not to be in agreement with this theory. These are critical temperature measurements on thin lead films as a function of thickness which are in contrast to the behavior predicted theoretically. Many studies have been devoted to rationalizing the dependence of the superconducting critical temperature T_c on confinement and on the thin film thickness L [16–21]. In the past, the superconducting thin films were mostly amorphous while nowadays, with the advent of modern preparation techniques, also thin films with good crystalline order can be obtained. Early numerical studies [16] suggested a possible enhancement of T_c upon decreasing L although a mechanistic explanation has remained elusive. More recently, experiments on ordered thin films [20, 21], besides the above mentioned regime of enhancement upon reducing L , have also highlighted a second regime at lower (nanometric) thickness L , where, instead, T_c grows with increasing L . Travaglino and Zaccone in a recent paper [22] developed the first fully analytical theory of confinement effects on superconductivity of thin films in the framework of the simplified weak-coupling BCS formalism. The mathematical predictions were verified for experimental data of crystalline thin films and were able to reproduce the trend of T_c vs L , including the maximum of T_c at $L = L_c = (2\pi/n)^{1/3}$, where n is the concentration of free carriers. However, the simplified weak-coupling BCS formula is not quantitative for Pb (which is a strong-coupling material), and adjustable parameters are used in the comparison.

Furthermore, a new topological transition in the available momentum space was predicted to occur at the critical L_c value of thickness, which corresponds to the maximum in T_c vs L [22].

In this paper we formulate a generalized Eliashberg theory of strong-coupling superconductivity that takes into account effects of quantum confinement on the free carriers, as well as a realistic electron–phonon spectral density. For doing this, it is necessary to use a generalization of standard s-wave one-band Eliashberg theory [14], where we ignore effects of structural disorder. The new Eliashberg equations are more complex than the usual ones, because the normal density of states (DOS) cannot be approximated by its value at the Fermi level and this fact produces a change in the form of the Eliashberg equations. This new theory is shown to produce predictions which, for the first time, are in quantitative agreement with experimental data of Pb and Al thin films, with no adjustable parameters.

2. The mathematical framework

2.1. Eliashberg equations

The standard (infinite) one-band s-wave Eliashberg equations, when the Migdal theorem holds [23], are given in terms of the renormalization function $Z(i\omega_n)$ and the gap function $\Delta(i\omega_n)$ as [15, 24–29]:

$$\begin{aligned} \Delta(i\omega_n)Z(i\omega_n) &= \pi T \sum_{\omega_{n'}} \frac{\Delta(i\omega_{n'})}{\sqrt{\omega_{n'}^2 + \Delta^2(i\omega_{n'})}} [\lambda(i\omega_{n'} - i\omega_n) - \mu^*(\omega_c)\theta(\omega_c - |\omega_{n'}|)] \\ Z(i\omega_n) &= 1 + \frac{\pi T}{\omega_n} \sum_{\omega_{n'}} \frac{\omega_{n'}}{\sqrt{\omega_{n'}^2 + \Delta^2(i\omega_{n'})}} \lambda(i\omega_{n'} - i\omega_n) \end{aligned} \quad (1)$$

where $\theta(\omega_c - |\omega_{n'}|)$ is the Heaviside function, ω_c is a cut-off energy ($\omega_c > 3\Omega_{\max}$ where Ω_{\max} is the maximum phonon energy) [25], $\mu^*(\omega_c)$ is the Coulomb pseudopotential, $\lambda(i\omega_{n'} - i\omega_n)$ is a function related to the electron-boson spectral density $\alpha^2F(\Omega)$ through the relation

$$\lambda(i\omega_{n'} - i\omega_n) = 2 \int_0^\infty \frac{\Omega \alpha^2 F(\Omega) d\Omega}{\Omega^2 + (\omega_{n'} - \omega_n)^2}. \quad (2)$$

The strength of the electron–phonon coupling intensity is given by the electron–phonon coupling parameter $\lambda = 2 \int_0^\infty \frac{\alpha^2 F(\Omega) d\Omega}{\Omega}$.

In general, the Eliashberg equations are solved numerically with iterative method until numerical convergence is reached. The numerical procedure is quite simple in the formulation

on the imaginary axis, but much less so on the real axis. The critical temperature can be calculated either by solving an eigenvalue equation or, more easily, by giving a very small test value to the superconducting gap (for the Pb it is $\Delta = 1.34$ meV at $T = 0$ K so, for example, $\Delta(T) = 10^{-7}$ meV) and then by checking at which temperature the solution converges. In this way, a precision in the T_c value is obtained that is much higher than the experimental confidence interval.

If one removes the approximations of the infinite bandwidth and of taking the DOS equal to a constant (i.e. its value at the Fermi level), the Eliashberg equations are slightly more complex and they become four equations [25]. However, when $N(\varepsilon) = N(-\varepsilon)$ (the DOS is symmetrical with respect to the Fermi level) the situation is particularly simple because the non-zero self energy terms remain two, i.e. just the equations for $Z(i\omega_n)$ and $\Delta(i\omega_n)Z(i\omega_n)$ and they read as [30, 31]

$$\Delta(i\omega_n)Z(i\omega_n) = \pi T \sum_{\omega_{n'}} \frac{\Delta(i\omega_{n'})}{\sqrt{\omega_{n'}^2 + \Delta^2(i\omega_{n'})}} \left[\frac{N(i\omega_{n'}) + N(-i\omega_{n'})}{2} \right] \times [\lambda(i\omega_{n'} - i\omega_n) - \mu^*(\omega_c)\theta(\omega_c - |\omega_{n'}|)] \frac{2}{\pi} \arctan \left(\frac{W}{2Z(i\omega_{n'})\sqrt{\omega_{n'}^2 + \Delta^2(i\omega_{n'})}} \right) \quad (3)$$

$$Z(i\omega_n) = 1 + \frac{\pi T}{\omega_n} \sum_{\omega_{n'}} \frac{\omega_{n'}}{\sqrt{\omega_{n'}^2 + \Delta^2(i\omega_{n'})}} \left[\frac{N(i\omega_{n'}) + N(-i\omega_{n'})}{2} \right] \lambda(i\omega_{n'} - i\omega_n) \times \frac{2}{\pi} \arctan \left(\frac{W}{2Z(i\omega_{n'})\sqrt{\omega_{n'}^2 + \Delta^2(i\omega_{n'})}} \right) \quad (4)$$

where $N(\pm i\omega_n) = N(\pm Z(i\omega_n)\sqrt{(\omega_n)^2 + \Delta^2(i\omega_n)})$ and the bandwidth W is equal to half the Fermi energy, $E_F/2$.

The fact of having a symmetric DOS is crucial otherwise it becomes much more complicated to arrive at numerical convergence.

2.2. Electron confinement model

When the system is confined along one of the three spatial directions, such as in thin films, the DOS cannot be approximated by a constant but takes a different form [22]. In this case, we have two different regimes depending on the film thickness L : in the first confinement regime, when $L > L_c$ and $E_F > \varepsilon^*$, the DOS has the following form

$$N(\varepsilon) = N(0)C \left[\vartheta(\varepsilon^* - \varepsilon) \sqrt{\frac{E_F}{\varepsilon^*} \frac{|\varepsilon|}{E_F}} + \vartheta(\varepsilon - \varepsilon^*) \sqrt{\frac{|\varepsilon|}{E_F}} \right]$$

where $C = (1 + \frac{1}{3} \frac{L_c^3}{L^3})^{1/3}$, $\varepsilon^* = \frac{2\pi^2 \hbar^2}{mL^2}$, $L_c = (\frac{2\pi}{n_0})^{1/3}$, m is the electron mass, L is the film thickness, n_0 is the density of carriers and $E_{F,bulk}$ is the Fermi energy of the bulk material. In this case, it is possible to demonstrate [22] the following relations:

$$E_F = C^2 E_{F,bulk} \quad (5)$$

$$N(E_F) = CN(E_{F,bulk}) = CN(0) \quad (6)$$

$$N(E_{F,bulk}) = \frac{V(2m)^{3/2}}{2\pi^2 \hbar^3} \sqrt{E_{F,bulk}} \quad (7)$$

In the second confinement regime, $L < L_c$, the DOS has a new, linear dependence on the energy, in contrast with the standard square-root dependence [22].

To summarize, in this version of the Eliashberg theory, four things will change:

(a) the DOS will no longer be a constant but a function of energy. We removed the factors C because we put this factor in the renormalization of the electron–phonon interaction so the DOS that we put in the Eliashberg equations in the first confinement regime $L > L_c$ is

$$N(\varepsilon) = \left[\vartheta(\varepsilon^* - \varepsilon) \sqrt{\frac{E_F}{\varepsilon^*} \frac{|\varepsilon|}{E_F}} + \vartheta(\varepsilon - \varepsilon^*) \sqrt{\frac{|\varepsilon|}{E_F}} \right] \quad (8)$$

(b) the electron–phonon interaction will be renormalized so as to have a new $\lambda = C\lambda^{bulk}$ in a way to scale the electron–phonon spectral function without changing its shape. We moved the factor of the normal DOS C inside the definition of electron–phonon coupling as in the Coulomb pseudopotential. Of course the reason for this choice is only pedagogic, because in this way we can justify the use of the Allen–Dynes equation [32] for T_c which is a crude, but effective, approximation of the numerical solution of the Eliashberg equations.

(c) the value of the Fermi energy will be renormalized in the following way: $E_F = C^2 E_{F,bulk}$. Furthermore, in the Eliashberg equations, in the symmetric case discussed above, it is $W = E_F/2$.

(d) the Coulomb pseudopotential changes (also the Fermi energy in the definition, changes):

$$\mu^* = \frac{C\mu_{bulk}}{1 + \mu_{bulk} \ln(E_F/\omega_c)}$$

$$\text{where } \mu_{bulk} = \frac{\mu_{bulk}^*}{1 - \mu_{bulk}^* \ln(E_{F,bulk}/\omega_c)}.$$

In the second confinement regime, when $L < L_c$ and $E_F < \varepsilon^*$ [22]:

$$N(\varepsilon) = C'N(0) \sqrt{\frac{E_F}{\varepsilon^*} \frac{\varepsilon}{E_F}} \quad (9)$$

where

$$N(\varepsilon = E_F) = C' N(0)$$

$$E_F = \frac{\hbar^2}{m} \sqrt{\frac{(2\pi)^3 n}{L}} = C'^2 E_{F,\text{bulk}}$$

$$C' = \frac{2}{\sqrt{L}} \left(\frac{8\pi}{3}\right)^{2/3} \frac{1}{(n(2\pi)^3)^{1/6}}.$$

In this confinement regime ($L < L_c$), the DOS is given by [22]:

$$N(\varepsilon) = \sqrt{\frac{E_F |\varepsilon|}{\varepsilon^* E_F}},$$

and the factor C' goes to renormalize the electron–phonon coupling and the Coulomb pseudopotential as follows:

$$\lambda = C' \lambda^{\text{bulk}}, \quad \mu^* = \frac{C' \mu_{\text{bulk}}}{1 + \mu_{\text{bulk}} \ln(E_F/\omega_c)}. \quad (10)$$

By recalling that in the Eliashberg equations the reference energy is the Fermi energy taken as the zero of the energy, in the program that numerically solves the Eliashberg equations, the DOS has been rescaled in the following way (by also putting care that the DOS is continuous for $\varepsilon = \varepsilon^*$). When $L > L_c$ and $\varepsilon^* < E_F$:

$$N(\varepsilon) = \left[\vartheta(\varepsilon^* - \varepsilon) \sqrt{\frac{E_F}{E_F - \varepsilon^*}} \left(1 - \frac{|\varepsilon|}{E_F}\right) + \vartheta(\varepsilon - \varepsilon^*) \left(1 - \sqrt{\frac{|\varepsilon|}{E_F}}\right) \right]. \quad (11)$$

Instead, when $L < L_c$ and $\varepsilon^* > E_F$:

$$N(\varepsilon) = \sqrt{\frac{E_F}{\varepsilon^*}} \left(1 - \frac{|\varepsilon|}{E_F}\right). \quad (12)$$

3. Comparison with experimental data

Now we can apply this theory to reproduce experimental data from the literature. The first set of experimental data refers to crystalline thin lead films [20, 21]. We further noticed that the T_c value for the maximum thickness is around 6.05 K that is somewhat different from the most quoted bulk value of 7.22 K. On the other hand, measurements performed on 500 monolayers thick films indeed show the bulk value for T_c , suggesting the possible existence of a 3D to quasi-2D transition [21]. We thus assume that the critical reference temperature is equal to 6.05 K. The bulk electron phonon spectral function [15] with $\lambda_{\text{bulk},0} = 1.55$ is shown in the inset of figure 1 and is that of Pb appropriately rescaled (we choose $\lambda^{\text{bulk}} = 1.3335$) to obtain, using the bulk value of the Coulomb pseudopotential $\mu^*(\omega_c) = 0.1338$ (the cut-off energy is $\omega_c = 90$ meV and the maximum electronic energy is $\omega_{\text{max}} = 100$ meV), the value of $T_c = 6.05$ K for $L = 50$ Å. The values [22] of the bulk Fermi

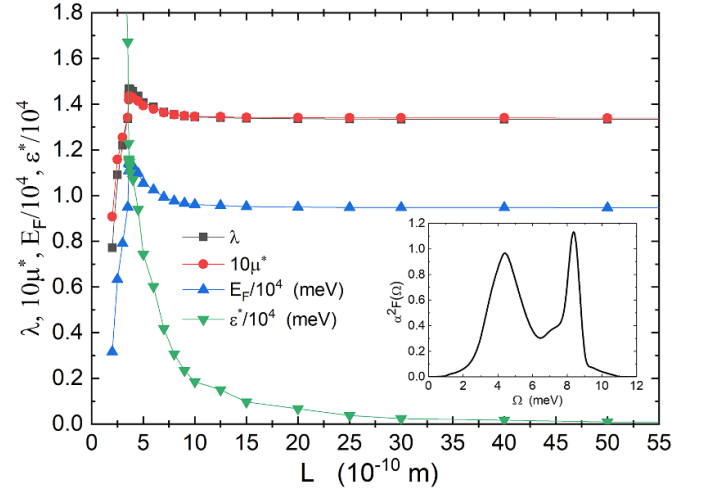


Figure 1. Theoretical parameters (λ (dark line), $10\mu^*$ (red line), $E_F/10^4$ (blue line), $\varepsilon^*/10^4$) versus film thickness for Pb thin films. For the calculations we assume a bulk electron–phonon coupling $\lambda^{\text{bulk}} = 1.337$ to obtain the experimental value [21] $T_c(L = 50 \text{ \AA}) = 6.05$ K. The true value of bulk electron–phonon coupling is $\lambda^{\text{bulk}} = 1.55$ and $T_c(L = \infty) = 7.22$ K. In the inset the bulk electron–phonon spectral function is shown [15]. The bulk Fermi energy is $E_{F,\text{bulk}} = 9470$ meV and we use the correct value of Coulomb pseudopotential for the bulk $\mu_b^* = 0.1338$.

energy and carrier density are respectively $E_{F,\text{bulk}} = 9470$ meV and $n_0 = 0.132 \cdot 10^{30} \text{ m}^{-3}$. This produces a critical thickness $L_c = 3.6$ Å. In figure 1 some typical physical quantities used in the theory are shown as functions of the film thickness.

We have solved the Eliashberg equations in a numerical way for determining the critical temperature of films of different thickness: the result is shown in figure 2. This calculation has no free parameters. Looking at figure 2 it might seem that the calculated critical temperature diverges but this is not the case. The maximum T_c is obtained by setting $L = L_c$ and, since the corresponding electron–phonon coupling, as can be seen in figure 1, is finite, so is the T_c which will be $T_{c,\text{max}} = 19.57$ K. In figure 3, the gap values versus temperature for three different film thickness: $L = 50$ Å (dark solid line), $L = 6$ Å (blue solid line) and $L = 3$ Å (red solid line) are shown.

We now can reproduce other experimental data from the literature relative to thin aluminum films [33]. The bulk electron phonon spectral function [34] with $\lambda_{\text{bulk},0} = 0.43$ [15] is shown in the inset of figure 4 while the bulk value of the Coulomb pseudopotential is chosen to be $\mu^*(\omega_c) = 0.14295$ (the cut-off energy is $\omega_c = 190$ meV and the maximum electronic energy is $\omega_{\text{max}} = 200$ meV), in order to produce the value of $T_{c,\text{bulk}} = 1.20$ K. The values of the bulk Fermi energy and carriers density are respectively [35] $E_{F,\text{bulk}} = 11700$ meV and $n_0 = 0.181 \cdot 10^{30} \text{ m}^{-3}$. This produces a critical thickness $L_c = 3.3$ Å. We can see that the theory with this value of free carrier concentration does not work (black solid line) in comparison with the experimental data [33]. The reason is that, in thin aluminum films, the carriers density is, actually, a few orders of magnitude lower than the above quoted bulk value $n_0 = 0.181 \cdot 10^{30}$ [36]. If we assume that, in Al thin films, the

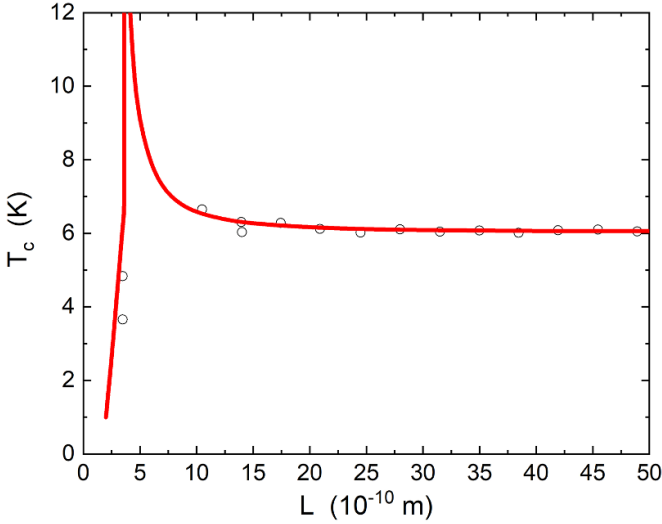


Figure 2. Experimental critical temperature versus film thickness: open circles represent experimental data for Pb thin films taken from [21], while the solid red line represents the theory of this paper. The apparent divergence at $L = L_c = 3.6 \text{ \AA}$ is due to the occurrence of a topological transition of the Fermi surface as predicted in [22]. One should note that the two data points corresponding to the two lowest L values refer to two different surface patterns in the experimental setup of [21].

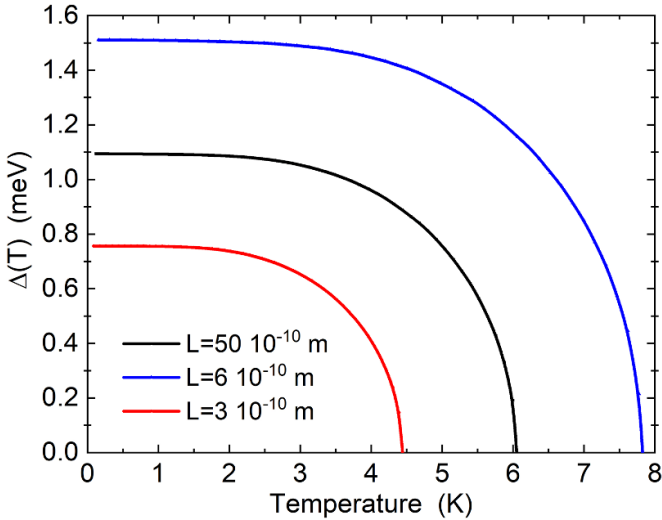


Figure 3. Calculated gap value versus temperature for three different film thickness: $L = 50 \text{ \AA}$ (dark solid line), $L = 6 \text{ \AA}$ (blue solid line) and $L = 3 \text{ \AA}$ (red solid line). All the other parameters are those used for Pb thin films in figures 1 and 2.

value of carriers density is $n_0 = 0.130 \cdot 10^{25} \text{ m}^{-3}$ ($L_c = 169.1 \text{ \AA}$), which is not far from experimental observations ($n_0 \sim 10^{25} \text{ m}^{-3}$ found in [36] for nanometric thin films, or even lower in [37]), we then obtain the red solid line in figure 4 that provides an excellent agreement with the experimental data. Even for aluminium, looking at figure 4 one might think that the calculated critical temperature diverges. Proceeding as in the previous case, i.e. placing $L = L_c$ in the Eliashberg equations, we find $T_{\text{cmax}} = 1.76 \text{ K}$.

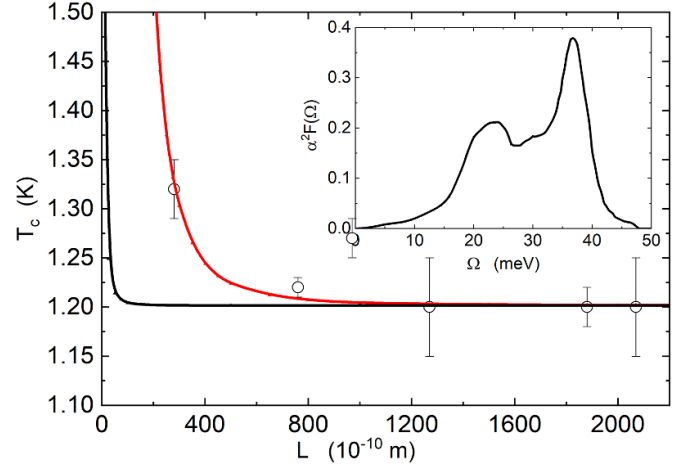


Figure 4. Critical temperature versus film thickness for Al thin films: open circles are experimental data from measurements of López-Núñez *et al* [33], the solid black line is the theory with $n_0 = 0.181 \cdot 10^{-30} \text{ m}^{-3}$ and the solid red line is the theory with $n_0 = 0.130 \cdot 10^{25} \text{ m}^{-3}$. In the inset, the Eliashberg electron-phonon spectral function is shown [15].

The penetration depth or the density of superfluid is another experimentally accessible physical quantity that can be also calculated within the two-band Eliashberg model, so as to further check the reliability of its predictions. The penetration depth of the magnetic field $\lambda(T)$ in the London limit [38] is expressed, without considering the anisotropy, as

$$\lambda^{-2}(T) = \left(\frac{\hbar \omega_p}{c} \right)^2 \pi k_B T \quad (13)$$

$$\times \sum_{n=-\infty}^{+\infty} \frac{\Delta_i^2(\omega_n) Z_i^2(\omega_n)}{[\omega_n^2 Z_i^2(\omega_n) + \Delta_i^2(\omega_n) Z_i^2(\omega_n)]^{3/2}} \quad (14)$$

where c is the speed of light, $Z(\omega_n)$ and $\Delta(\omega_n)$ are the solutions of the Eliashberg equations and $\omega_p \propto E_F^{3/4}$ is the plasma frequency [35]. The results for the superfluid density $n_s \propto \lambda^{-2}$ are shown in figure 5 for the same thickness values used in figure 3. It is clear that $n_s \propto \lambda^{-2}$ increases markedly with increasing the film thickness L . This theoretical prediction is in qualitative agreement with recent experimental data of [33] where the magnetic penetration depth λ is observed to decrease markedly upon increasing L .

4. Absence of oscillations in T_c vs L

A gas of free electrons inside a rectangular slab (box) is described by basic quantum mechanics in terms of plane waves with a wavefunction $\psi \sim \sin(k_x x) \sin(k_y y) \sin(k_z z)$ obeying the Schrödinger equation. Here, z could be the confined dimension. This form of wavefunction, as is well known, arises from ‘hard-wall’ boundary conditions (BCs), i.e. upon imposing that the wavefunction is identically null exactly at the boundaries of the box. Furthermore, the plane waves of the quantum particles in a 3D isotropic sample in real space, must satisfy

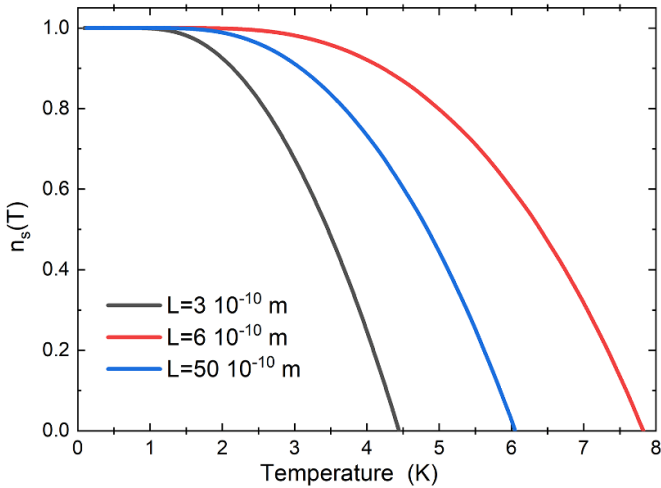


Figure 5. Calculated normalized density of superfluid $n_s \propto \lambda^{-2}$ versus temperature T for three different film thickness values: $L = 50 \text{ \AA}$ (blue solid line), $L = 6 \text{ \AA}$ (red solid line) and $L = 3 \text{ \AA}$ (black solid line). All the other parameters are those used for Pb thin films in figures 1 and 2.

the following relation in reciprocal space [39, 40]:

$$\frac{1}{k^2} (k_x^2 + k_y^2 + k_z^2) = 1, \quad (15)$$

with $|\mathbf{k}| = k = 2\pi/\lambda$ the modulus of the wavevector \mathbf{k} , and λ is the wavelength. While k_x, k_y, k_z are, in general, discretized for small systems owing to the hard-wall BCs, or periodic BCs, and to the wave-like character of the Schrödinger equation, if the sample is, instead, macroscopically extended in the xy plane, k can still be treated as a quasi-continuous variable. Also, it is important to recognize that the hard-wall BCs are a strong idealization of the real physical system, where atomic-scale roughness, disorder and irregularities prevent the wavefunctions to become exactly null at a fixed coordinate, thus making k_z not a good quantum number [41]. Indeed, as it is well known from quantum mechanics, momentum is a good quantum number for hard-wall or periodic BCs, but not for open BCs [42], the latter being much more realistic for real-world thin films due to the atomic roughness and irregularities of the interface. Hence, while oscillations as a function of the number of atomic layers are often observed in numerical simulations, they are not usually visible in the experimental data [43]. This is due to the more regular atomic-scale structure of simulated thin films compared to experimental ones, especially at the interface; and also because the total number of atoms in the experimental samples is typically much larger than in simulations (since they are much more extended in the lateral directions). This, in turn, makes the distribution of occupied momentum states in experimental systems behave in a more continuum-like manner, which makes the oscillations in measured properties not visible. As a result of all these facts, it was observed in [44] (cf the supplementary information therein), that, on the example of phonons in ultra-thin ice films, there is no discretization of the wavevector k_z along the

confinement direction, even when the film thickness is lower than 1 nm.

The key fact that k_z is not discretized, for the reasons reported above, explains the absence of oscillations in the T_c vs L experimental data for both Pb and Al thin films presented above in figures 2 and 4. This is because, if k_z were discretized as a good quantum number, in the presence of hard-wall BCs, it would lead to strong oscillations in $g(E_F)$ vs L , which, in turn, would produce strong oscillations in T_c vs L . This is evident since, e.g. in the simplest BCS theory, $T_c \sim \exp(-\frac{1}{Ug(E_F)})$. This fact is well known from the numerical solutions obtained long ago by Blatt and Thompson [16], who numerically solved the BCS theory for thin films with a discretized k_z and vanishing BCs at the boundaries. Indeed, they obtained very large oscillations in their predicted Δ vs L , which are not supported by the experimental data. For a thorough discussion of these issues from the numerical point of view, we refer the interested readers to the recent work of Valentinis *et al* [18]. These authors found, indeed, that, for more realistic conditions, there are no oscillations in the T_c vs L behavior, in agreement with our theoretical predictions above.

5. Conclusions

We have provided a formulation of the Eliashberg theory of superconductivity in real solids, which, for the first time, accounts for quantum confinement effects on the electron states due to nanometric confinement in thin films. This theory, for the first time, has been shown here to be able to quantitatively predict the size-dependent superconducting critical temperature as a function of film thickness, with no adjustable parameters. The comparison has been successfully presented for two key real solids such as Pb and Al thin films, and the agreement is excellent. Theory also predicts that the magnetic field penetration depth decreases markedly with increasing the film thickness, in qualitative agreement with recent experimental data. This result opens up the way for unprecedented opportunities to quantitatively design and engineer superconducting thin films for a number of applications ranging from superconducting qubits, Dayem bridges, electric-field driven quantum gated devices and single-photon detectors.


Data availability statement

All data that support the findings of this study are included within the article (and any supplementary files).

Acknowledgments

G A U acknowledges partial support from the MEPhI. A Z gratefully acknowledges funding from the European Union through Horizon Europe ERC Grant Number: 101043968 ‘Multimech’, from US Army Research Office through Contract No. W911NF-22-2-0256, and from the Niedersächsische Akademie der Wissenschaften zu Göttingen in the frame of the Gauss Professorship program.

ORCID iDs

Giovanni Alberto Ummarino  <https://orcid.org/0000-0002-6226-8518>

Alessio Zaccone  <https://orcid.org/0000-0002-6673-7043>

References

- [1] Sklyadneva I Y, Heid R, Bohnen K-P, Echenique P M and Chulkov E V 2013 *Phys. Rev. B* **87** 085440
- [2] Brun C, Hong I-P, Patthey F m c, Sklyadneva I Y, Heid R, Echenique P M, Bohnen K P, Chulkov E V and Schneider W-D 2009 *Phys. Rev. Lett.* **102** 207002
- [3] Mishra K, Piquette A and Johnson K 2017 *J. Appl. Phys.* **122** 063104
- [4] Saniz R, Partoens B and Peeters F M 2013 *Phys. Rev. B* **87** 064510
- [5] van Weerdenburg W M J, Kamlapure A, Fyhn E H, Huang X, van Mullekom N P E, Steinbrecher M, Krogstrup P, Linder J and Khajetoorians A A 2023 *Sci. Adv.* **9** eadf5500
- [6] Nguyen D-L, Wei C-M and Chou M-Y 2019 *Phys. Rev. B* **99** 205401
- [7] Huang G Q 2008 *Phys. Rev. B* **78** 214514
- [8] Bouchiat V, Faucher M, Thirion C, Wernsdorfer W, Fournier T and Pannetier B 2001 *Appl. Phys. Lett.* **79** 123
- [9] You L *et al* 2018 *Opt. Express* **26** 2965
- [10] Oliver W D and Welander P B 2013 *MRS Bull.* **38** 816–25
- [11] De Simoni G, Paolucci F, Strambini E and Giazotto F 2018 *Nat. Nanotechnol.* **13** 802
- [12] De Simoni G, Paolucci F, Puglia C and Giazotto F 2019 *ACS Nano* **13** 7871–6
- [13] Zaccone A and Fomin V M 2024 *Phys. Rev. B* **109** 144520
- [14] Eliashberg G M 1960 *Sov. Phys.-JETP* **11** 696
- [15] Carbotte J P 1990 *Rev. Mod. Phys.* **62** 1027
- [16] Blatt J M and Thompson C J 1963 *Phys. Rev. Lett.* **10** 332
- [17] Arutyunov K Y *et al* 2019 *Phys. Solid State* **61** 1559
- [18] Valentinis D, van der Marel D and Berthod C 2016 *Phys. Rev. B* **94** 054516
- [19] Bianconi A and Missori M 1994 *J. Physique I* **4** 361
- [20] Eom D, Qin S, Chou M-Y and Shih C K 2006 *Phys. Rev. Lett.* **96** 027005
- [21] Qin S, Kim J, Niu Q and Shih C-K 2009 *Science* **324** 1314
- [22] Travaglino R and Zaccone A 2023 *J. Appl. Phys.* **133** 033901
- [23] Ummarino G A and Gonnelli R S 1997 *Phys. Rev. B* **56** R14279
- [24] Marsiglio F and Carbotte J P 2008 Electron-phonon superconductivity *Superconductivity: Conventional and Unconventional Superconductors* ed K H Bennemann and J B Ketterson (Springer) pp 73–162
- [25] Allen P B and Mitrović B 1983 *Theory of Superconducting T_c* (Academic) pp 1–92
- [26] Parks R D (ed) 1969 *Superconductivity* vol 1 (Marcel Dekker) p 67
- [27] Marsiglio F 1992 *J. Low Temp. Phys.* **87** 659
- [28] Ummarino G 2013 Eliashberg theory *Emergent Phenomena in Correlated Matter* ed E Pavarini, E Koch and U Schollwoeck (Forschungszentrum Jülich GmbH and Institute for Advanced Simulations) pp 13.1–36
- [29] Margine E R and Giustino F 2013 *Phys. Rev. B* **87** 024505
- [30] Schachinger E and Carbotte J P 1983 *J. Phys. F: Met. Phys.* **13** 2615
- [31] Pickett W E 1980 *Phys. Rev. B* **21** 3897
- [32] Allen P B and Dynes R C 1975 *Phys. Rev. B* **12** 905
- [33] López-Núñez D, Montserrat Q P, Rius G, Bertoldo E, Torras-Coloma A, Martínez M and Forn-Díaz P 2023 Magnetic penetration depth of aluminum thin films (arXiv:2311.14119 [cond-mat.supr-con])
- [34] Liu A Y and Quong A A 1996 *Phys. Rev. B* **53** R7575
- [35] Ashcroft N and Mermin N 1976 *Solid State Physics* (Holt-Saunders)
- [36] Du H, Gong J, Sun C, Lee S W and Wen L S 2004 *J. Mater. Sci.* **39** 2865
- [37] Schaub A, Slepíčka P, Kašpárková I, Malinský P, Macková A and Švorčík V 2013 *Nanoscale Res. Lett.* **8** 249
- [38] Golubov A, Brinkman A, Dolgov O V, Kortus J and Jepsen O 2002 *Phys. Rev. B* **66** 054524
- [39] Hill T L 1960 *An Introduction to Statistical Thermodynamics* (Addison-Wesley) pp 493–5
- [40] Kittel C 2005 *Introduction to Solid State Physics* 8th edn (Wiley)
- [41] Elliott S 1990 *Physics of Amorphous Materials* (Longman)
- [42] Desai B R 2009 *Quantum Mechanics With Basic Field Theory* (Cambridge University Press)
- [43] Wan W, Yao Y, Sun L, Liu C-C and Zhang F 2017 *Adv. Mater.* **29** 1604788
- [44] Yu Y, Yang C, Baggioli M, Phillips A E, Zaccone A, Zhang L, Kajimoto R, Nakamura M, Yu D and Hong L 2022 *Nat. Commun.* **13** 3649